

Starburst Intensity Limit of Galaxies at $z \simeq 5-6$

N. P. Hathi¹, S. Malhotra^{1,2} and J. E. Rhoads^{1,2}

Nimish.Hathi@asu.edu

ABSTRACT

The peak star formation intensity in starburst galaxies does not vary significantly from the local universe to redshift $z \sim 6$. We arrive at this conclusion through new surface brightness measurements of 47 starburst galaxies at $z \simeq 5-6$, doubling the redshift range for such observations. These galaxies are spectroscopically confirmed in the Hubble Ultra Deep Field (HUDF) through the GRISM ACS program for Extragalactic Science (GRAPES) project. The starburst intensity limit for galaxies at $z \simeq 5-6$ agree with those at $z \simeq 3-4$ and $z \simeq 0$ to within a factor of a few, after correcting for cosmological surface brightness dimming and for dust. The most natural interpretation of this constancy over cosmic time is that the same physical mechanisms limit starburst intensity at all redshifts up to $z \simeq 6$ (be they galactic winds, gravitational instability, or something else). We do see two trends with redshift: First, the UV spectral slope (β) of galaxies at $z \simeq 5-6$ is bluer than that of $z \simeq 3$ galaxies, suggesting an increase in dust content over time. Second, the galaxy sizes from $z \simeq 3$ to $z \simeq 6$ scale approximately as the Hubble parameter $H^{-1}(z)$. Thus, galaxies at $z \simeq 6$ are high redshift starbursts, much like their local analogs except for slightly bluer colors, smaller physical sizes, and correspondingly lower overall luminosities. If we now assume a constant maximum star formation intensity, the differences in observed surface brightness between $z \simeq 0$ and $z \simeq 6$ are consistent with standard expanding cosmology and strongly inconsistent with tired light model.

Subject headings: galaxies: high redshift — galaxies: starburst

1. Introduction

Star formation on galactic scales is a key ingredient in understanding galaxy evolution. We cannot compare structure formation calculations to observed galaxy populations without

¹Department of Physics, Arizona State University, Tempe, AZ 85287-1504, USA

²School of Earth and Space Exploration, Arizona State University, Tempe, AZ 85287-1404, USA

some model for how star formation proceeds. Such models are based on detailed observations in the nearby universe, combined with physically motivated scaling for differing conditions elsewhere in the universe. To test the validity of such scaling, it is valuable to directly measure the properties of star formation events in the distant universe, and see how they compare with their nearby counterparts.

Starbursts are regions of intense massive star formation that can dominate a galaxy’s integrated spectrum. By comparing the properties of starbursts over a wide range of redshifts, we can test whether the most intense star formation events look the same throughout the observable history of the universe. High redshift galaxies are expected, on average, to be less massive and lower in metal abundance than their present-day counterparts. Either effect could in principle change the maximum intensity of star formation that such galaxies can sustain.

Meurer et al. (1997) (hereafter M97) measured the effective surface brightness, i.e., the average surface brightness within an aperture that encompasses half of the total light, for various samples. They conclude that the maximum effective surface brightness of starburst galaxies is unchanged to better than an order of magnitude out to redshifts $z \simeq 3$. Weedman et al. (1998) (hereafter W98) measured observed surface brightness from the single brightest pixel and concluded that high-redshift ($2.2 \lesssim z \lesssim 3.5$) starburst galaxies have intrinsic ultra-violet (UV) surface brightnesses that are typically 4 times higher than for low-redshift starburst galaxies. Both M97 and W98 measured their surface brightness for spectroscopically confirmed galaxies in the Hubble Deep Field (HDF; Williams et al. 1996).

We have measured the surface brightness of starburst regions at $3 \lesssim z \lesssim 6$, using photometry from the Hubble Ultra Deep Field (HUDF) images (Beckwith et al. 2006) and redshifts from the GRISM ACS Program for Extragalactic Science (GRAPES) project (PI S. Malhotra; Pirzkal et al. 2004). We combine these with earlier published results comparing $z \simeq 3$ and $z \simeq 0$ starbursts (M97, W98). The starburst intensity limit of starburst regions at $5 \lesssim z \lesssim 6$ sample is consistent with that at $z \simeq 3$ and $z \simeq 0$ to within the uncertainties, which are about a factor of three. *These high redshift star forming regions are thus starbursts, with a star formation intensity similar to their local counterparts despite any effects of differing metallicity and/or galaxy size.* The starbursts should then be a set of standard surface brightness objects, and can be used to apply Tolman’s test for expansion of the universe (Tolman 1930, 1934) over an unprecedented redshift range ($0 < z \lesssim 6$). Our surface brightness observations fully support standard expanding universe models. This result is robust to even rather large systematic errors, thanks to the wide redshift range spanned by the data.

This paper is organized as follows: In § 2 we summarize the HUDF and the GRAPES observations, and we present details of the sample selection. In § 3 we describe our data

analysis to measure the UV spectral slope and the effective surface brightness of starburst galaxies following the method used by M97, in § 4 we apply the pixel based method of W98 to estimate the limiting surface brightness for our galaxies, in § 5 we discuss measurement biases that will affect our surface brightness measurements, and our results of the starburst intensity limit, the size evolution & the change in the UV spectral slope. Finally, in § 6 we summarize our results.

Throughout this paper we denote the *HST*/ACS F435W, F606W, F775W and F850LP filters as B , V , i' , z' , *HST*/WFPC2 F814W as I and *HST*/NIC3 F110W and F160W as J and H -bands, respectively. We assume a *Wilkinson Microwave Anisotropy Probe* (WMAP) cosmology of $\Omega_m=0.24$, $\Omega_\Lambda=0.76$ and $H_0=73 \text{ km s}^{-1} \text{ Mpc}^{-1}$, in accord with the recent 3 year WMAP estimates of Spergel et al. (2007). This implies an age for the Universe of 13.7 Gyr. Magnitudes are given in the AB system (Oke & Gunn 1983).

2. Observational Data and Sample Selection

The HUDF is a 400 orbit survey of a $3.4' \times 3.4'$ field carried out with the ACS in the B , V , i' and z' filters (see Beckwith et al. 2006, for further details). We have carried out deep unbiased slitless spectroscopy of this field with the ACS grism as part of the GRAPES project, which was awarded 40 HST orbits during Cycle 12 (ID 9793; PI S. Malhotra). The grism observations were taken at four different orientations in order to minimize the spectra contamination and overlapping from nearby sources. We have extracted useful low resolution spectra ($R \simeq 100$) from 5900Å to 9500Å for many sources in the HUDF down to a limiting magnitude of $z'_{\text{AB}} \simeq 27.5$ in the AB system. Details of the observations, data reduction and final GRAPES catalog are described in a paper by Pirzkal et al. (2004).

We identify high-redshift galaxies on the basis of their ACS grism spectra. This identification was based on detecting the Lyman break in the continuum or the $\text{Ly}\alpha$ emission for these sources. With the ACS grism low-resolution spectra, we are able to determine the redshifts to an accuracy of $\Delta z \approx 0.15$ even for the faintest detectable Lyman Break Galaxies (LBGs) ($z'_{\text{AB}} \simeq 27.5$). Details of the selection process are described in Malhotra et al. (2005). There are 47 star-forming galaxies at $z \simeq 5-6$ in the GRAPES/HUDF with confirmed spectroscopic redshifts. These redshifts are sufficiently high that rest-frame flux measurements are available for UV wavelengths comparable to those at which M97 and W98 measured the surface brightness of starburst regions at $z \lesssim 3$. We used the following spectroscopically confirmed samples for our analysis.

- The $z \simeq 3$ LBGs from the Hubble Deep Field (HDF, Giavalisco et al. 1996; Steidel et al.

1996a,b) were used to compare our measurements with M97. This sample of 10 galaxies at $z \simeq 3$ forms the subset of UV samples used by M97. We measured the UV spectral slopes (β) using observed ($V-I$) and ($G-R$) colors, and rest-frame UV fluxes were derived from the observed R -band (combined V and I light) magnitudes (Giavalisco et al. 1996; Steidel et al. 1996a,b).

- The $z \simeq 4$ B -band dropout galaxies were selected from the VLT redshift catalog of Vanzella et al. (2006). This sample is small (4 galaxies), but is useful for comparing $z \simeq 3-4$ and $z \simeq 5-6$ galaxy samples. We used the observed ($i'-z'$) color to estimate β , and rest-frame UV fluxes were derived from the observed z' -band magnitudes. The observed i' - and z' -band magnitudes for $z \simeq 4$ galaxies were obtained from the HUDF catalogs of Beckwith et al. (2006).
- We use a sample of 47 $z \simeq 5-6$ starburst galaxies having GRAPES redshifts (Malhotra et al. 2005; Rhoads et al. 2007, in preparation) in the HUDF. Table 1 shows properties (coordinates, magnitudes, sizes and redshifts) for these 47 galaxies. We further selected a subset of 19 galaxies covered by the Thompson et al. (2005) HUDF NICMOS images. We estimate β from the observed ($J-H$) color. The rest-frame UV fluxes were derived from the observed J and H -band magnitudes for 19 galaxies, while the average β is used to predict J and H -band magnitudes for the remaining 28 galaxies.

3. Starburst Intensity Limit Using M97 Approach

3.1. Magnitudes and Color Measurements

All measurements for galaxies at $z \simeq 4-6$ were done on the HST ACS HUDF images (Beckwith et al. 2006) and HST NICMOS images (Thompson et al. 2005). The HST NICMOS images were reprocessed by L. Eddie Bergeron (private communication). The HST NICMOS images cover $\sim 50\%$ of the HUDF ACS field. Therefore, only half of our galaxies have J - and H -band imaging. We need J and H magnitudes for galaxies at $z \simeq 5-6$ to measure the UV spectral slopes and luminosities at $\sim 2200\text{\AA}$ rest-frame. We use rest-frame $\sim 2200\text{\AA}$ to measure the effective surface brightness for consistency with M97. All broad-band magnitudes are measured as `SExtractor` (Bertin & Arnouts 1996) `MAG_AUTO` magnitudes, using dual-image mode to generate aperture matched catalogs. We use the z' -band image as the detection image. `MAG_AUTO` apertures are Kron-like (Kron 1980) flexible apertures and they enclose most of the flux for an object. These apertures are same in all filters for a given object. We also measured `SExtractor` Petrosian (1976) magnitudes (`MAG_PETRO`), with $\eta=0.2$ (Holwerda 2005), and isophotal magnitudes (`MAG_ISO`). We find

that the average difference between `MAG_AUTO` and `MAG_PETRO` is ~ 0.1 mag, while the average difference between `MAG_AUTO` and `MAG_ISO` is ~ 0.2 mag. The effect of this magnitude uncertainty on the surface brightness measurements is very small (< 0.1 dex). Our method to measure magnitudes is the same for all galaxies at $z \simeq 4-6$, and is consistent with the curve-of-growth method used for our comparison sample of $z \simeq 3$ galaxies (Giavalisco et al. 1996; Steidel et al. 1996a,b). We use `MAG_AUTO` magnitudes to calculate the UV spectral slope (β) and the effective surface brightness.

3.2. The UV Spectral Slope (β)

The UV spectral slope (β) is determined from a power-law fit to the UV continuum spectrum (Calzetti et al. 1994),

$$f_\lambda \propto \lambda^\beta ,$$

where f_λ is the flux density per unit wavelength ($\text{ergs s}^{-1} \text{cm}^{-2} \text{\AA}^{-1}$). Converting this into magnitude units yields a linear relationship between β and colors. Figure 1 shows the average values of the UV spectral slopes, β , for galaxies at $z \simeq 3-4$ and $z \simeq 5-6$. The mean values are plotted with error bars indicating the standard deviation of the mean (i.e. the sample standard deviation (σ) divided by the square root of the sample size (N)). The UV slopes for 10 galaxies at $z \simeq 3$ are obtained using the following two equations (M97) for two slightly different samples:

$$\beta = 2.55 \cdot (G - R) - 2 \quad \text{and} \quad \beta = 3.23 \cdot (V - I) - 2 .$$

Here G and R filters are defined in Steidel & Hamilton (1993). We also plot the average β measured for 4 galaxies at $z \simeq 4$, using:

$$\beta = 5.65 \cdot (i' - z') - 2$$

where we have used pivot wavelengths for i' - and z' -band, $\lambda_{i'}=7693\text{\AA}$ and $\lambda_{z'}=9055\text{\AA}$, respectively, to obtain the slope of 5.65 in β -color linear relationship. Figure 1 also shows the average β for 19 galaxies at $z \simeq 5-6$ obtained using

$$\beta = 2.56 \cdot (J - H) - 2$$

where we have used pivot wavelengths for J - and H -band, $\lambda_J=11200\text{\AA}$ and $\lambda_H=16040\text{\AA}$, respectively, to obtain the slope of 2.56 in β -color linear relationship. We do not use ($z'-J$) color to estimate β for galaxies at $z \simeq 5-6$ because, the ($z'-J$) colors can be insensitive to rest-frame UV colors due to the shorter color baseline and are also more sensitive to uncertainties in the optical to infrared zero points (Bouwens et al. 2006). Therefore for

comparison, we also measured β for galaxies at $z \simeq 5$ using $(i'-z')$ colors and found that the average β is -1.53 ± 0.38 compared to -1.65 ± 0.21 , the average β at $z \simeq 5$ using $(J-H)$ colors. This comparison implies that small variations in the UV rest-frame wavelength and observed colors does not affect the slope within the quoted uncertainties.

Figure 1 shows that the average β decreases from -1.13 ± 0.17 at $z \simeq 3$ to -1.74 ± 0.35 at $z \simeq 6$. The change in the average slope shows that the galaxies at $z \simeq 5-6$ are bluer than those at $z \simeq 3$, but redder than the flat slope in f_ν ($f_\lambda \propto \lambda^{-2}$), that would be expected for a dust-free starburst galaxy.

3.3. Half-Light Radius (r_e) Measurements

The half-light radius is defined as the radius containing 50% of the total flux of an object. The half-light radii for galaxies at $z \simeq 3$ are derived by Giavalisco et al. (1996) & Steidel et al. (1996b) and are measured such that half of the total emission from the starburst is enclosed within a circular aperture. We used the **SExtractor** half-light radii (R50, radii enclosing 50% of the flux within a circular aperture) obtained from the HUDF z' -band catalog (Beckwith et al. 2006) for galaxies at $z \simeq 4-6$. All radii are converted from arcsecs to kpc using a WMAP cosmology in the cosmological calculator by Wright (2006). The half-light radii for galaxies at $z \simeq 4-6$ are measured at rest-frame UV wavelengths $\lambda = 1500 \pm 300 \text{ \AA}$. The sizes do not change appreciably when measured within this wavelength range. Figure 2 shows the average values of the half-light radii for 10 starburst galaxies at $z \simeq 3$, 4 starburst galaxies at $z \simeq 4$, and 47 starburst galaxies at $z \simeq 5-6$. Mean half-light radii are plotted with error bars indicating the standard deviation of the mean. The solid and dashed curves show the trend if sizes evolve as $H^{-1}(z)$ or $H^{-2/3}(z)$, respectively, where $H(z)$ is the Hubble parameter at redshift z . The curves are normalized to the mean size we measure at $z \simeq 4$ ($\sim 0.21''$ or ~ 1.5 kpc). Comparison between galaxies at $z \simeq 3$ and $z \simeq 5-6$ shows that the galaxy sizes increase as we go from $z \simeq 6$ to $z \simeq 3$.

We independently measured various flavors of **SExtractor** radii (half-light, Petrosian (1976), Kron) for galaxies at $z \simeq 5-6$ to assess the differences in these measurements. The Petrosian radius is defined as the radius at which the surface brightness is certain factor (η) of the average surface brightness within this isophote, while the Kron radius is defined as the typical size of the flexible aperture computed from the moments (see **SExtractor** manual by Holwerda 2005, for further details). The difference in the average values of the half-light and the other two radii was approximately $\pm 0.04''$. Therefore, we expect about 30% uncertainty in the measurements of the half-light radii for galaxies at $z \simeq 5-6$.

3.4. Calculation of Surface Brightness for Starburst Galaxies

We measure the effective surface brightness for 14 starburst galaxies at $z \simeq 3-4$ and 47 starburst galaxies at $z \simeq 5-6$ by adopting the method used by M97. First, we need to estimate dust extinction A_{1600} and k -corrections from the UV spectral slope (β). Dust extinction is estimated using the linear empirical relation between A_{1600} and β (Meurer et al. 1999), which is given by following equation:

$$A_{1600} = 4.43 + 1.99 \cdot (\beta)$$

where A_{1600} is the net absorption in magnitudes by dust at 1600\AA .

The next step in correcting apparent flux for corresponding rest-frame UV flux is to apply, where appropriate, the k -correction. We use following equation to estimate k -correction (M97):

$$k = \frac{f_{2320}}{f_{\lambda_c/1+z}} = \left[\frac{(1+z) \cdot 2320\text{\AA}}{\lambda_c} \right]^\beta$$

where λ_c corresponds to the central wavelength of the filters used for the observed flux. Here we reference all observations to the observations in M97, which has UV central wavelength of 2320\AA . We apply above mentioned dust and k -corrections to apparent magnitudes to estimate absolute magnitudes and intrinsic UV luminosities for our samples of $z \simeq 3-6$ galaxies. The ratio of intrinsic UV to bolometric luminosity can be calculated for young starbursts. By using the stellar population models of Bruzual & Charlot (2003) to convert from intrinsic F220W flux/luminosity to bolometric luminosity, we find that the ratio of the UV to bolometric luminosity changes due to variations in the metallicity and the dust attenuation. The luminosity ratio spans a range from ~ 0.2 to ~ 0.5 . The adopted ratio of the intrinsic UV to bolometric luminosity is:

$$\frac{L}{L_{\text{bol}}} \simeq 0.33$$

We are using this value for the UV to bolometric luminosity ratio for two reasons: (1) this bolometric correction is very close to the average value we get from our stellar population models and (2) this correction factor is also predicted by the models used by M97.

From L_{bol} and the half-light radii (r_e), we calculate effective surface brightness (S_e) using following relation:

$$S_e = \frac{L_{\text{bol}}}{2\pi r_e^2} \left(\frac{L_\odot}{\text{kpc}^2} \right) .$$

Here r_e is measured in kpc and L_{bol} in solar luminosities (L_\odot).

To characterize the S_e distribution for all galaxies in our sample we consider the median and 90th percentiles, which we denote as $S_{e,50}$ and $S_{e,90}$, respectively. The upper limit to the surface brightness (starburst intensity limit) of starbursts is traced by $S_{e,90}$. Here we have used average β (from Figure 1) for each sample to estimate the surface brightness. Figure 3 shows L_{bol} and S_e as a function of r_e for the $z \simeq 0-6$ galaxy samples. The $z \simeq 0$ and $z \simeq 0.4$ surface brightness measurements are taken from M97. The $z \simeq 0$ data point is the median measurement for 11 nearby galaxies. The $S_{e,50}$ and $S_{e,90}$ surface brightness levels of the combined sample are plotted as dashed and dotted lines respectively.

The top panel of the Figure 3 shows that the bolometric luminosities for galaxies at $z \simeq 5-6$ are smaller than the luminosities of galaxies at $z \simeq 3$. Using a two-sided K-S test on these luminosity distributions, we reject the hypothesis that the $z \simeq 3$ and $z \simeq 5-6$ luminosities are drawn from the same population at $>99\%$ probability. From the bottom panel of Figure 3, it is apparent that S_e shows little or no dependence on r_e over about one order of magnitude in size; hence there is no dependence on L_{bol} over about two orders of magnitude in luminosity. Figure 4 shows the effective surface brightness (S_e) as a function of redshift. The $z \simeq 0$ and $z \simeq 0.4$ surface brightness measurements are taken from M97. From Figure 3 and Figure 4, we find that $S_{e,90}$ of the starbursts remains constant (within uncertainties) with redshift.

4. Starburst Intensity Limit Using W98 Approach

We also studied the surface brightnesses using the brightest pixel approach pioneered by Weedman et al. (1998). Weedman et al. (1998) measures observed surface brightness of the brightest pixel for galaxies at $2.2 \lesssim z \lesssim 3.5$ in the HDF and compared with the local starbursts by fading their observed (f_λ) surface brightness by $(1+z)^{-5}$. We use this approach to compare surface brightnesses of the brightest pixel for galaxies at $z \simeq 3-6$.

A postage stamp (51×51 pixels) for each galaxy at $z \simeq 5-6$ was excised from the z' -band HUDF image. Using z' -band segmentation maps, only object pixels were selected. For each object pixel in the postage stamp, we estimate the apparent magnitude. For the brightest pixel in each galaxy, the average UV spectral slope β was used to predict J -band (for galaxies at $z \simeq 5$) and H -band (for galaxies at $z \simeq 6$) magnitudes from z' -band apparent magnitudes. Using similar approach as discussed in § 3.4, we calculated the intrinsic UV luminosity (L_\odot^{UV}) for the brightest pixel in each galaxy at $z \simeq 5-6$. For surface brightness measurements, we divide the intrinsic UV luminosity by the area of one pixel in kpc^2 .

Figure 5 shows surface brightness ($L_\odot^{\text{UV}} \text{kpc}^{-2}$) for the brightest pixel in each of the 47

galaxies at $z \simeq 5-6$ and 4 galaxies at $z \simeq 4$. We have also plotted 18 galaxies at $z \simeq 3$ from W98. The W98 galaxies has observed surface brightnesses for the brightest pixels and hence, for proper comparison, we converted observed surface brightnesses for W98 galaxies to their corresponding rest-frame surface brightnesses. Here we have used average β for $z \simeq 3$ galaxies as shown in Figure 1, to estimate extinction and k -correction. The median ($S_{bp,50}$) and 90th percentile ($S_{bp,90}$) surface brightness levels of the combined sample are plotted as dashed and dotted lines, respectively. Here, the starburst intensity limit of starbursts is traced by $S_{bp,90}$. The $S_{bp,90}$ of galaxies at $z \simeq 3$ and $z \simeq 5-6$ is same to within a factor of ~ 0.10 dex.

We cannot properly compare the brightest pixel surface brightnesses between the W98 sample at $z \simeq 0$ and galaxies at $z \simeq 3-6$ for two reasons. First, the aperture sizes for W98 galaxies at $z \simeq 0$ are larger than the physical sizes corresponding to one pixel at $z \simeq 3-6$, and the sizes for W98 galaxies at $z \simeq 0$ are also larger than the effective radii measured by Meurer et al. (1995) for some of these local galaxies. Second, the discrepancy between the W98 adopted UV spectral slope (β) and β from Meurer et al. (1995) is large for some of these galaxies, which affects the applied extinction for their luminosity measurements.

The effective surface brightness approach of M97 (§ 3) and the brightest pixel approach of W98 suggests that the starburst intensity limit, as defined by $S_{e,90}$ or $S_{bp,90}$, of the starbursts is unchanged (within uncertainties) from $z \simeq 5-6$ down to $z \simeq 3$.

5. Results and Discussion

5.1. Selection and Measurement Effects

Different radii-measurements. — The results shown in Figures 2 and 4 use **SExtractor** half-light radii derived by Beckwith et al. (2006). Here we discuss the uncertainty in the surface brightness measurements due to radii measurements. We use three different flavors of radii measured using **SExtractor**. We measured the half-light radii, the Petrosian (1976) radii and the Kron radii for galaxies at $z \simeq 5-6$. We found that the average difference between the half-light radius and other two radii was approximately $\pm 0.04''$. This difference does not affect our conclusion that $z \simeq 5-6$ galaxies are smaller compared to $z \simeq 3$ galaxies. As shown in Figure 2, the average value of the half-light radii for galaxies at $z \simeq 5-6$ is $0.14''$ compared to $0.32''$ which is the average value for galaxies at $z \simeq 3$. The uncertainty in three different radii measurements is $\pm 0.04''$. Therefore for a given luminosity, we expect that this difference in radii measurement will cause ~ 0.2 dex difference in $S_{e,90}$ estimate.

Surface brightness selection. — The limiting surface brightness in the HUDF samples is $S_e \sim 5.0 \times 10^9 L_\odot \text{ kpc}^{-2}$ at $z \simeq 5-6$, which is much fainter than the observed maximum

surface brightness ($S_{e,90} \simeq 2.3 \times 10^{11} L_{\odot} \text{ kpc}^{-2}$) for all galaxies. At low surface brightness limit our sample could be incomplete but at the maximum surface brightness level our sample is complete.

Size selection effect. — The $z \simeq 3$ galaxies are spectroscopically confirmed by Keck observations. The limiting magnitude for Keck spectroscopy is $R \lesssim 25.3$ (Steidel et al. 1996b). Using $S_{e,90}$ and the limiting magnitude, we estimate the minimum observable size for this sample as ~ 700 pc or $\sim 0.1''$. Therefore, this sample of galaxies at $z \simeq 3$ is not biased against smaller sizes.

Flux uncertainty. — Here we discuss three possible sources of uncertainties in the magnitudes (for a given size) that will affect our surface brightness measurements. They are as follows: (1) The average **SExtractor** uncertainties in J , H magnitudes are ~ 0.2 mag. The largest magnitude uncertainties in the sample range up to ~ 0.5 mag for three objects. Even this worst case magnitude uncertainty affects $S_{e,90}$ by only ~ 0.2 dex. The uncertainty in $S_{e,90}$ due to the average difference between various magnitudes (**MAG_AUTO**, **MAG_PETRO** and **MAG_ISO**) is very small (< 0.1 dex) and hence the magnitude uncertainty dominates the uncertainty in $S_{e,90}$. (2) The ratio of the UV to bolometric luminosity for starburst galaxies is based on the stellar population models. We find that this ratio is affected by the change in metallicity or dust extinction in the stellar population models. The uncertainty in this ratio can be as large as a factor of ~ 2.0 . This uncertainty in the bolometric correction will change $S_{e,90}$ estimate by ~ 0.3 dex but this is systematic uncertainty and will affect all starburst galaxies. (3) We have used linear fit to the observed relation between the F_{FIR}/F_{1600} and the UV spectral slope (β) to estimate A_{1600} (Fig.1 in Meurer et al. 1999). The scatter in this plot can cause an uncertainty in A_{1600} of ~ 0.4 mag. This uncertainty in A_{1600} will change $S_{e,90}$ estimate by ~ 0.2 dex. This uncertainty will systematically affect all galaxies in this study.

Therefore, if these logarithmic uncertainties add in quadrature, we would expect the total uncertainty in $S_{e,90}$ to be ~ 0.5 dex.

5.2. The Starburst Intensity Limit

We measure the effective surface brightness (S_e) and the brightest pixel surface brightness (S_{bp}) of the *spectroscopically* confirmed galaxies at $z \simeq 5-6$ in the HUDF and compare with the spectroscopically confirmed galaxies at $z \simeq 3$ in the HDF. We conclude that to better than a factor of 3, the starburst intensity limit of starbursts at $z \simeq 3$ and $z \simeq 5-6$ are the same. Using the K-S test on these distributions, the resulting probabilities ($\gtrsim 20\%$) support

the hypothesis that these distributions are drawn from the same population. By combining the samples at $z \simeq 3\text{--}4$ and $z \simeq 5\text{--}6$, we find a mean $S_{e,90} \simeq 2.3 \times 10^{11} L_{\odot} \text{ kpc}^{-2}$ (with a factor of 3 or ~ 0.5 dex uncertainty). We quantify the scatter in the S_e and S_{bp} distributions (Figure 5 and 6) by measuring standard deviation (σ) from a Gaussian fit to these distributions. We find that the scatter in the S_e distribution ($\sigma_{\log(S_e)} \simeq 0.37$) is higher than the scatter in the S_{bp} distribution ($\sigma_{\log(S_{bp})} \simeq 0.27$). Therefore, the brightest pixel method could be very useful in estimating the starburst intensity limit of starburst galaxies.

The approximate constancy of peak starburst intensity can be interpreted as the evidence that the interstellar medium (ISM) can only support some maximum pressure. Heckman et al. (1990) used [S II] emission line ratios to determine the ISM pressure (P_0) for a sample of galaxies (mostly starbursts) undergoing a strong galactic wind. The star formation intensity required to produce P_0 is $S_e \simeq 1.7 \times 10^{11} L_{\odot} \text{ kpc}^{-2}$ (M97). This value agrees closely with our $S_{e,90}$ but derived using different method. The physical process can be explained by assuming that the ISM pressure provides a “thermostat” for star formation, such that strong outflows will result whenever the pressure rises above P_0 and shut down further star formation for a time. This results in a characteristic peak starburst intensity. We convert $S_{e,90}$ to an equivalent star formation intensity ($M_{\odot} \text{ yr}^{-1} \text{ kpc}^{-2}$) by using conversion factors between UV luminosity and star formation rate from Kennicutt (1998) and M97. We get star formation intensity in the range of $30\text{--}50 M_{\odot} \text{ yr}^{-1} \text{ kpc}^{-2}$ depending on the conversion factor. This peak intensity is physically distinct from the minimum intensity required to produce a galactic wind, which is orders of magnitude lower, at $\sim 0.1 M_{\odot} \text{ yr}^{-1} \text{ kpc}^{-2}$ (Lehnert & Heckman 1996; Heckman 2001). Thus, *every* galaxy in our sample is expected to have a wind, as Lehnert et al. (2007) remark for a similar sample of $z \gtrsim 3$ Lyman break galaxies. However, only in galaxies near the starburst intensity limit does the “thermostat” become active.

While the peak starburst intensity stays constant with redshift, the dust optical depth that we infer from the observed spectral slope β decreases systematically with redshift. This suggests that the star formation intensity limit does not depend on dust content, at least over the range of dust optical depths $\tau_{dust} \gtrsim 1$ probed by our sample. At yet higher redshifts we might expect that $\tau_{dust} < 1$, and that the starburst radiation field would no longer couple efficiently to the interstellar medium. Whether this would substantially change the starburst intensity limit would depend on the fraction of starburst wind driving that is due to radiation pressure rather than stellar winds and mechanical energy from supernova explosions.

The constancy of maximum star-formation surface intensity with redshift provides a basis for a strong test of the expanding Universe. Standard cosmologies predict that the bolometric surface brightness should vary with redshift as $(1+z)^{-4}$. Our results (using

standard cosmology) combined with M97 results at low redshifts show that the maximum star formation intensity remains constant (within uncertainties) from $z \simeq 0$ to $z \simeq 6$. This conclusion depends critically on the use of a standard cosmology to go from observed flux and radius to inferred star formation intensity. Thus, if the peak star formation rate per unit area is controlled by some physical limit that is based on local, redshift-independent physics, our observations essentially require standard surface brightness dimming. While other evolutionary effects could become important, we have minimized these by measuring surface brightnesses at nearly fixed rest wavelength. Had we instead taken a “tired light” model, where bolometric surface brightness falls off as $(1+z)^{-1}$, our observations would require the true star formation intensity to be dramatically lower at high redshift— by a factor of order $(1+z)^3 \sim 7^3 \sim 300$. This factor greatly exceeds the estimated uncertainties in our analysis. Hence, the wide redshift range of our sample yields a strong application of Tolman’s (Tolman 1930, 1934) test, and we derive strong evidence in favor of the expanding Universe and against any alternative “tired light” models.

5.3. Size and Luminosity Evolution

An average galaxy at $z \simeq 5-6$ in our sample has half-light radii of ~ 0.8 kpc or $\sim 0.14''$, as shown in Figure 2, which is in good agreement with a number of recent studies (Bouwens et al. 2004, 2006; Pirzkal et al. 2007; Dow-Hygelund et al. 2007). Ferguson et al. (2004) compares sizes of galaxies at $z \simeq 1-5$ within a fixed luminosity range. Our results agree with Ferguson et al. (2004) for $z \simeq 3-4$. The UV intrinsic luminosities for our sample of galaxies are brighter or equal to L^* (i.e. $L \gtrsim L^*$) at respective redshifts but we do not require any particular minimum luminosity, while Ferguson et al. (2004) do require a minimum luminosity. Given that surface brightness is near-constant, a minimum luminosity immediately implies some minimum radius for inclusion in the Ferguson et al. (2004) sample. Figure 2 also shows comparison of our size measurements with the Ferguson et al. (2004) and the Bouwens et al. (2006) results. The solid and dashed curves in the Figure 2 show the trend if sizes evolve as $H^{-1}(z)$ or $H^{-2/3}(z)$, respectively, where $H(z)$ is the Hubble parameter at redshift z . The curves are normalized to the mean size we measure at $z \simeq 4$ ($\sim 0.21''$ or ~ 1.5 kpc). The galaxy sizes from $z \simeq 3$ to $z \simeq 6$ scale approximately as the Hubble parameter $H^{-1}(z)$, though it is difficult to conclude with certainty how sizes scale from the measurements of high redshift ($z \gtrsim 3$) galaxies only, because two trends diverge significantly at lower redshifts ($z < 3$).

We also find that the bolometric or intrinsic UV luminosity for galaxies at $z \simeq 5-6$ is lower than for galaxies at $z \simeq 3-4$. The galaxies at $z \simeq 5-6$ are smaller compared to $z \simeq 3$

galaxies, while the surface brightness as measured in § 3.4 remains approximately constant. Therefore, the luminosity evolution could be due to the constant upper limit on the surface brightness as a function of redshift.

5.4. Evolution in UV Spectral Slope (β)

Our $z \simeq 3-6$ sample also allows us to place constraints on the rest-frame UV slope. We obtained these constraints by measuring rest-frame UV colors of $z \simeq 3-4$ and $z \simeq 5-6$ galaxies as shown in Figure 1. A comparison of our measured colors with those obtained in two previous studies (Stanway et al. 2005; Bouwens et al. 2006) show agreement within our 1σ uncertainties. The mean β inferred from this study for $z \simeq 6$ galaxies is $\beta = -1.74 \pm 0.35$, which is redder than the $\beta = -2.0 \pm 0.3$ inferred in the Bouwens et al. (2006) or the $\beta = -2.2 \pm 0.2$ inferred in the Stanway et al. (2005). We also find that the mean β value for galaxies at $z \simeq 5-6$ is bluer than the $\beta = -1.1 \pm 0.2$ we measure at $z \simeq 3$ or the $\beta = -1.5 \pm 0.4$ observed by the Adelberger & Steidel (2000). Irrespective of the exact β , the mean rest-frame UV slope observed at $z \simeq 5-6$ is bluer than that observed at $z \simeq 3$. This evolution is consistent with number of recent studies (Stanway et al. 2005; Yan et al. 2005; Bouwens et al. 2006).

To understand the evolution in the β , we use the `STARBURST99` stellar synthesis code *version 5.1* (Leitherer et al. 1999; Vázquez & Leitherer 2005) to investigate the variations in β as function of IMF, metallicity and the star formation history. We assume two different metallicities ($Z = 0.004$ and 0.02), two different star formation histories (constant and instantaneous) and two different versions of the Salpeter (1955) IMFs ($\alpha = 2.35$ with $M_{up} = 100 M_{\odot}$ and $\alpha = 2.35$ with $M_{up} = 30 M_{\odot}$). We measure β for various models by fitting a first-order polynomial to the UV spectra through the wavelength interval $1250-1850 \text{ \AA}$. We find that the changes in metallicity and the IMF have much smaller effect on the rest-frame UV slope for young ($\lesssim 20$ Myr) starbursts. Our results agree with the Leitherer et al. (1999) models showing that the UV spectral slopes are independent of evolution and IMF effects. Leitherer et al. (1999) shows that for young starbursts, the UV spectral slope (β) at 2500 \AA also does not change very much as a function of model parameters (Z and IMF). Therefore the observed evolution in β from $z \simeq 5-6$ to $z \simeq 3$ is more likely due to the change in the dust content.

6. Summary

We have measured the starburst intensity limit for *spectroscopically confirmed* galaxies at $z \simeq 5-6$ from ACS grism survey GRAPES in the HUDF. We find that there is little

variation in the surface brightness from $z \simeq 3$ to $z \simeq 6$ and the starburst intensity limit is within a factor of 3 when compared with the sample of $z \simeq 3-4$ galaxies. The constancy of starburst intensity limit for starburst galaxies at $z \simeq 5-6$ combined with the results obtained by M97 for starbursts at $z \lesssim 3$ implies that the physical processes limiting starburst intensity at lower redshifts also apply to these high redshift galaxies. We find that the high redshift starbursts have a smaller characteristic linear size than their local counterparts, and a correspondingly lower luminosity (since their surface brightnesses are similar, and their sizes smaller). We observe the galaxy size evolution from $z \simeq 3$ to $z \simeq 6$ and find that the sizes scale approximately as the Hubble parameter $H^{-1}(z)$. Finally, using rest-frame UV colors we conclude that the evolution in the UV spectral slope from $z \simeq 3$ to $z \simeq 6$ reinforces the dust evolution which leads to bluer galaxies at $z \simeq 5-6$ compared to galaxies at $z \simeq 3$. This implies that starbursts were less obscured when the universe was younger and had lower heavy element abundances. Any future search for galaxies at higher redshifts (e.g. *James Webb Space Telescope (JWST)*; Windhorst et al. 2007) needs to take into account the size evolution & constancy of surface brightness; therefore the decrease in characteristic luminosity with redshift.

We would like to thank Rogier Windhorst, Rolf Jansen and Seth Cohen for providing useful comments on earlier drafts of this paper. This work was supported by grants GO 9793 and GO 10530 from the Space Telescope Science Institute, which is operated by AURA under NASA contract NAS5-26555. We also thank the anonymous referee for helpful suggestions that improved the paper.

REFERENCES

- Adelberger, K. L., & Steidel, C. C. 2000, *ApJ*, 544, 218
- Beckwith, S., et al. 2006, *AJ*, 132, 1729
- Bertin, E., & Arnouts, S. 1996, *A&AS*, 117, 393
- Bouwens, R. J., Illingworth, G. D., Blakeslee, J. P., Broadhurst, T. J., & Franx, M. 2004, *ApJ*, 611, 1
- Bouwens, R. J., Illingworth, G. D., Blakeslee, J. P., & Franx, M. 2006, *ApJ*, 653, 53
- Bruzual, G., & Charlot, S. 2003, *MNRAS*, 344, 1000
- Calzetti, D., Kinney, A. L., & Storchi-Bergmann, T. 1994, *ApJ*, 429, 582

- Dow-Hygelund, C. C., et al. 2007, *ApJ*, 660, 47
- Eyles, L. P., Bunker, A. J., Stanway, E. R., Lacy, M., Ellis R. S., & Doherty, M. 2005, *MNRAS*, 364, 443
- Ferguson, H. C., et al. 2004, *ApJ*, 600, L107
- Giavalisco, M., Steidel, C. C., & Macchetto, F. D. 1996, *ApJ*, 470, 189
- Heckman, T. M., Armus, L., & Miley, G. K. 1990, *ApJS*, 74, 833
- Heckman, T. M., Lehnert, M. D., Strickland, D. K., & Armus, L. 2000, *ApJS*, 129, 493
- Heckman, T. M. 2001, in *ASP Conf. Ser. 240, Gas and Galaxy Evolution*, ed. J. E. Hibbard, M. Rupen, & J. H. van Gorkom (San Francisco: ASP), 345
- Holwerda, B. W. 2005, ([astro-ph/0512139](#))
- Kennicutt, R. C., Jr. 1998, *ARA&A*, 36, 189
- Kron, R. G. 1980, *ApJS*, 43, 305
- Lehnert, M. D., & Heckman, T. 1996, *ApJ* 472, 546
- Lehnert, M. D., Bremer, M., Verma, A., Douglas, L., & Forster Schreiber, N. 2007, in *ASP Conf. Ser., Pathways Through an Eclectic Universe*, ed. J. H. Knappen, T. J. Mahoney, & A. Vazdekis ([astro-ph/0708.3000](#))
- Leitherer, C., et al. 1999, *ApJS*, 123, 3
- Malhotra, S., et al. 2005, *ApJ*, 626, 666
- Meurer, G. R., Heckman, T. M., Leitherer, C., Kinney, A., Robert, A., & Garnett, D. R. 1995, *AJ*, 110, 2665
- Meurer, G. R., Heckman, T. M., Lehnert, M. D., Leitherer, C., & Lowenthal, J. 1997, *AJ*, 114, 54 (M97)
- Meurer, G. R., Heckman, T. M., & Calzetti, D. 1999, *ApJ*, 521, 64
- Oke, J. B., & Gunn, J.E. 1983, *ApJ*, 266, 713
- Petrosian, V. 1976, *ApJ*, 209, L1
- Pirzkal, N., et al. 2004, *ApJS*, 154, 501

- Pirzkal, N., Malhotra, S., Rhoads, J., & Xu, C. 2007, ApJ, in press (astro-ph/0612513)
- Salpeter, E. E. 1955, ApJ, 121, 161
- Spergel, D. N., et al. 2007, ApJS, 170, 377
- Stanway, E. R., McMahon, R. G., & Bunker, A. J. 2005, MNRAS, 359, 1184
- Steidel, C. C., & Hamilton, D. 1993, AJ, 105, 2017
- Steidel, C. C., Giavalisco, M., Pettini, M., Dickinson, M., & Adelberger, K. L. 1996a, ApJ, 462, L17
- Steidel, C. C., Giavalisco, M., Dickinson, M., & Adelberger, K. L. 1996b, AJ, 112, 352
- Thompson, R. I., et al. 2005, AJ, 130, 1
- Tolman, R. C. 1930, PNAS, 16, 511
- Tolman, R. C. 1934, *Relativity, Thermodynamics, & Cosmology*, (Oxford: Oxford Univ. Press), 467
- Vanzella, E., et al. 2006, A&A, 454, 423
- Vázquez, G. A., & Leitherer, C. 2005, ApJ, 621, 695
- Weedman, D. W., Wolovitz, J. B., Bershad, M. A., & Schneider, D. P. 1998, AJ, 116, 1643 (W98)
- Williams, R. E., Blacker, B., Dickinson, M., et al. 1996, AJ, 112, 1335
- Windhorst, R. A., Hathi, N. P., Cohen, S.H., & Jansen, R. A. 2007, *Advances in Space Research*, in press (astro-ph/0703171)
- Wright, E. L. 2006, PASP, 118, 1711
- Yan, H., et al. 2005, ApJ, 634, 109

Table 1. Sample of $z \simeq 4-6$ Galaxies.

HUDF ID [†]	RA (J2000)	DEC (J2000)	<i>B</i> (mag)	<i>V</i> (mag)	<i>i'</i> (mag)	<i>z'</i> (mag)	<i>J</i> (mag)	<i>H</i> (mag)	R50* (pix)	<i>z</i> (GRAPES)
119	53.1660072	-27.8238735	28.98	29.22	27.46	27.83	3.42	5.09
322	53.1716057	-27.8207884	99.00	31.94	29.15	27.05	5.33	5.70
457	53.1627077	-27.8189684	99.00	33.04	29.77	28.36	4.00	5.80
865 §	53.1652728	-27.8140614	27.48	25.47	24.71	24.51	5.83	3.89 ‡
1115	53.1722701	-27.8119757	99.00	27.93	26.38	26.19	26.71	26.21	4.67	4.70
1392	53.1563542	-27.8095882	99.00	31.18	27.78	28.44	2.43	5.10
2225	53.1667243	-27.8041607	99.00	29.68	26.73	25.16	25.47	25.29	5.24	5.80
2285	53.1683346	-27.8041253	99.00	29.75	27.92	27.83	3.18	5.20
2408	53.1885344	-27.8034642	31.30	28.69	26.87	26.68	5.87	4.90
2599	53.1626591	-27.8022980	99.00	28.83	27.20	27.12	27.56	27.80	3.81	5.00
2631	53.1774780	-27.8024502	99.00	99.00	29.82	27.88	4.21	6.60
2690	53.1407464	-27.8021066	99.00	33.28	29.24	27.35	3.26	5.90
2881	53.1415939	-27.8005701	99.00	27.65	25.93	25.70	25.66	25.50	5.62	4.60
2894	53.1462479	-27.8008152	99.00	29.90	27.79	27.80	3.64	5.30
2898	53.1798235	-27.8008762	36.61	28.51	27.00	27.15	27.66	27.75	3.74	4.80
3250	53.1326635	-27.7989462	99.00	30.39	27.45	27.59	4.62	4.90
3317	53.1439706	-27.7986558	31.40	29.89	28.32	27.11	27.28	27.26	7.86	6.10
3325	53.1439441	-27.7988859	99.00	31.96	28.77	27.13	27.26	27.02	3.92	6.00
3377	53.1359748	-27.7984127	32.41	35.99	28.59	27.70	26.97	26.02	4.05	5.60
3398	53.1358677	-27.7983281	31.61	31.30	28.23	26.82	27.03	27.27	4.83	5.60
3450	53.1428483	-27.7978540	32.37	33.01	28.86	27.51	27.02	27.44	6.39	5.90
3503	53.1429396	-27.7982143	99.00	31.16	29.37	27.92	5.52	6.40
3807	53.1457274	-27.7966782	99.00	31.90	29.28	28.33	4.10	6.10
3968	53.1833352	-27.7959542	32.56	30.25	27.83	28.72	4.20	4.70
4050	53.1392840	-27.7957997	31.35	31.44	29.58	27.49	27.33	27.46	3.74	6.00
4173	53.1721175	-27.7950895	99.00	29.56	27.34	27.16	3.55	5.00
5307	53.1908539	-27.7903658	99.00	29.79	27.41	26.96	26.67	26.73	3.67	5.00
5788	53.1456512	-27.7882204	31.06	29.89	27.61	27.02	6.07	5.10
6329	53.1466545	-27.7861315	99.00	31.16	28.10	27.02	27.15	27.46	3.97	5.50
6515	53.1273683	-27.7851701	99.00	28.55	27.34	27.59	3.13	4.75
7050	53.1510303	-27.7828664	31.22	29.48	27.45	26.89	27.29	27.25	4.04	5.40
7352	53.1376952	-27.7812664	31.88	28.88	26.92	26.86	26.45	26.16	6.27	4.60
8033	53.1519631	-27.7781802	99.00	31.24	28.70	26.29	26.35	25.75	7.22	6.00
8301	53.1671739	-27.7745269	35.49	29.64	27.28	27.00	27.37	27.03	4.73	4.90
8664	53.1890679	-27.7770073	99.00	28.77	26.92	26.80	4.96	5.00
8682	53.1887985	-27.7770926	30.61	28.08	26.13	25.83	8.01	5.00
8896	53.1900057	-27.7790583	31.79	28.44	26.94	26.90	4.73	5.00
8961	53.1420611	-27.7797801	99.00	30.65	28.83	26.68	4.01	5.80
9202	53.1383610	-27.7786918	99.00	32.11	29.13	27.61	5.41	5.70
9409 §	53.1534403	-27.7661189	27.22	25.21	24.70	24.59	5.30	3.79 ‡
9777	53.1702380	-27.7628560	99.00	28.19	26.20	25.35	5.04	5.40
9857	53.1627716	-27.7607679	30.87	38.76	28.58	27.12	3.69	5.80
9983	53.1671618	-27.7598597	30.31	27.51	25.66	25.51	7.34	4.80
20191	53.1725568	-27.8137124	31.23	27.15	25.77	25.67	25.81	25.51	5.79	4.67
30591	53.1553196	-27.8151593	33.39	31.37	32.27	27.51	4.99	6.70

Table 1—Continued

HUDF ID [†]	RA (J2000)	DEC (J2000)	<i>B</i> (mag)	<i>V</i> (mag)	<i>i'</i> (mag)	<i>z'</i> (mag)	<i>J</i> (mag)	<i>H</i> (mag)	R50* (pix)	<i>z</i> (GRAPES)
32042	53.1689736	−27.8007244	99.00	32.72	31.75	28.84	4.00	5.75
33003	53.1460653	−27.7944931	99.00	99.00	31.63	28.00	27.47	27.35	4.01	6.40
35506	53.1660816	−27.7719653	30.31	32.92	31.06	27.82	5.97	6.20
36383	53.1677041	−27.7681044	99.00	99.00	31.07	28.66	5.58	5.80
−101 §	53.1770656	−27.7643556	26.23	24.52	24.20	24.22	7.50	3.60 ‡
−102 §	53.1431467	−27.8155017	27.95	25.10	24.17	24.14	9.70	4.14 ‡

[†]Identification from the HUDF catalogs of Beckwith et al. (2006), ACS grism spectra from Malhotra et al. (2005).

*Half light radius (R50) measured in *z'*-band.

§Objects from Beckwith et al. (2006) *B*-band dropout catalog. Two objects with negative IDs don't have published HUDF IDs.

‡Redshifts from Vanzella et al. (2006).

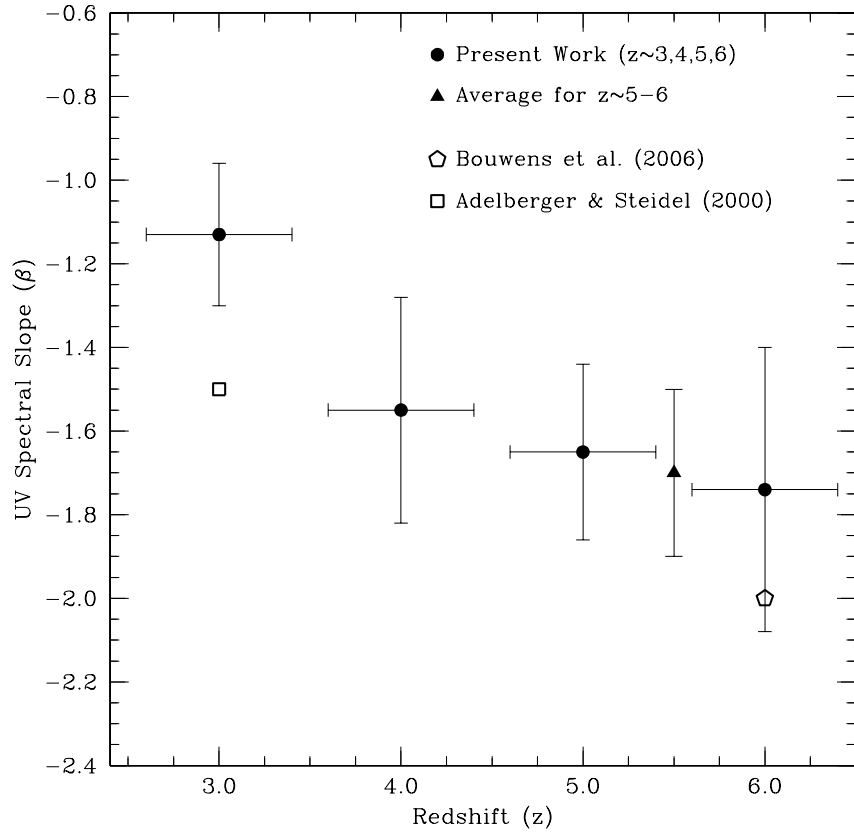


Fig. 1.— UV spectral slopes (β) v/s redshift relation. Mean β are plotted with error bars indicating the standard deviation of the mean (i.e. σ/\sqrt{N}). We have plotted the data points at $z \simeq 3$ from Adelberger & Steidel (2000) and at $z \simeq 6$ from Bouwens et al. (2006) for comparison.

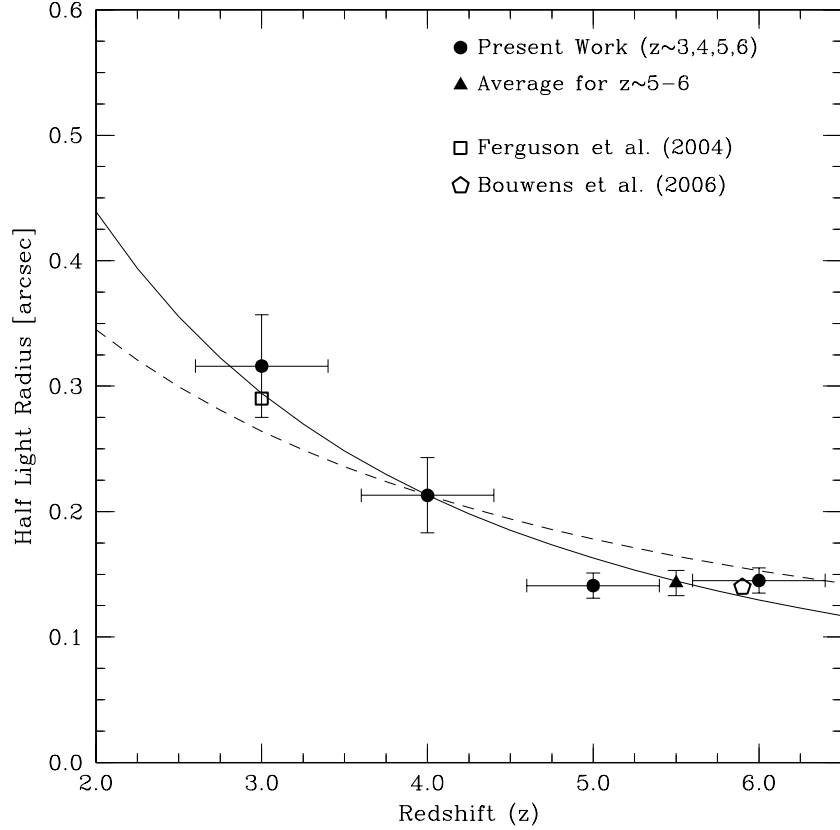


Fig. 2.— Size v/s redshift relation. Mean half-light radii are plotted with error bars indicating the standard deviation of the mean (i.e. σ/\sqrt{N}). The solid and dashed curves shows the trend if sizes evolve as $H^{-1}(z)$ and $H^{-2/3}(z)$, respectively. Both curves are normalized to the mean size at $z \simeq 4$ ($\sim 0.21''$ or ~ 1.5 kpc). We have plotted the data points at $z \simeq 3$ from Ferguson et al. (2004) and at $z \simeq 6$ from Bouwens et al. (2006) for comparison.

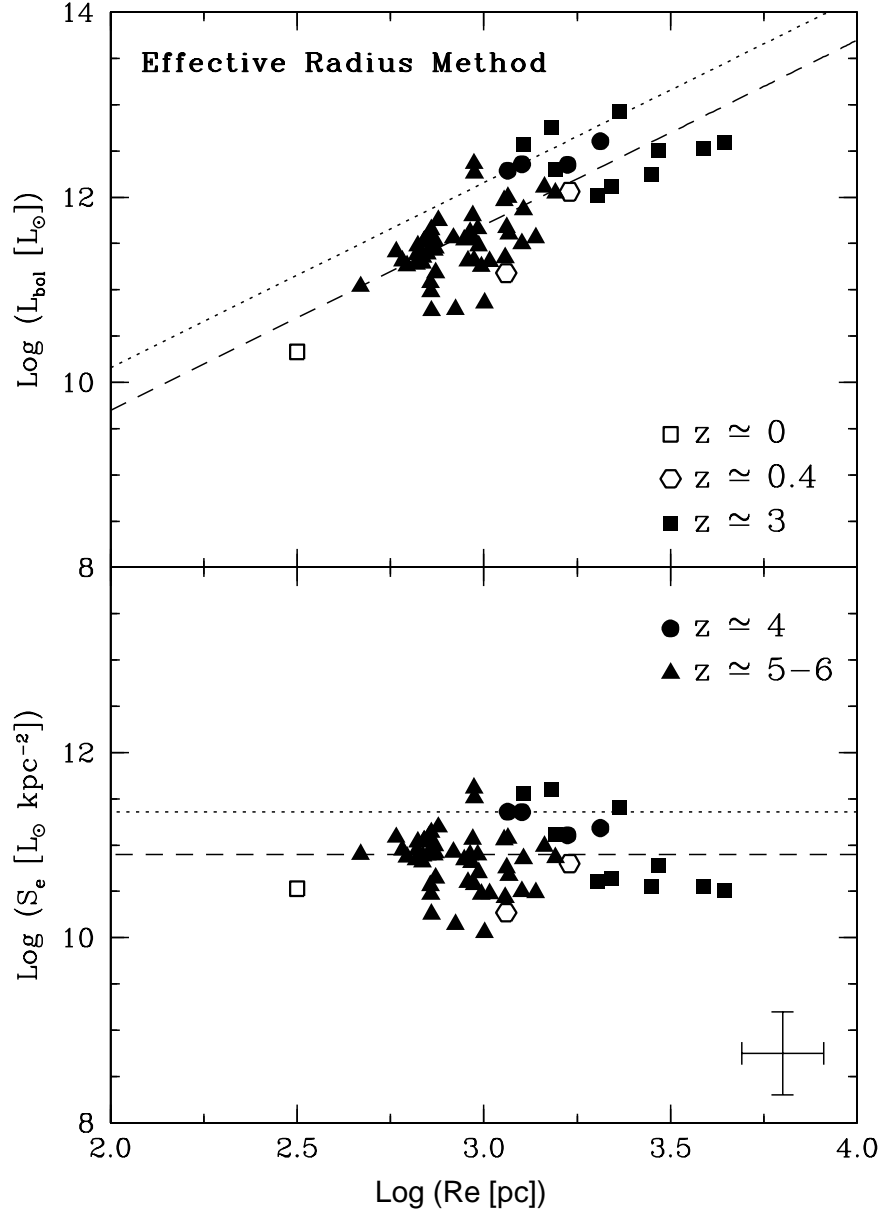


Fig. 3.— Bolometric luminosity (L_{\odot}^{bol}) and effective surface brightness ($L_{\odot}^{\text{bol}} \text{ kpc}^{-2}$) against effective radii for starburst galaxies. The filled squares, circles and triangles are measurements for galaxies at $z \approx 3$, $z \approx 4$ and $z \approx 5-6$, respectively. The open square ($z \approx 0$) is the median measurement of 11 nearby galaxies from M97. The open diamonds ($z \approx 0.4$) are S_e measurements from M97. The dotted and dashed lines correspond to $S_{e,90}$ and $S_{e,50}$ of the combine sample. Uncertainties in $z \approx 3-6$ surface brightness and radii measurements are shown in lower right corner, details are given in § 5.1.

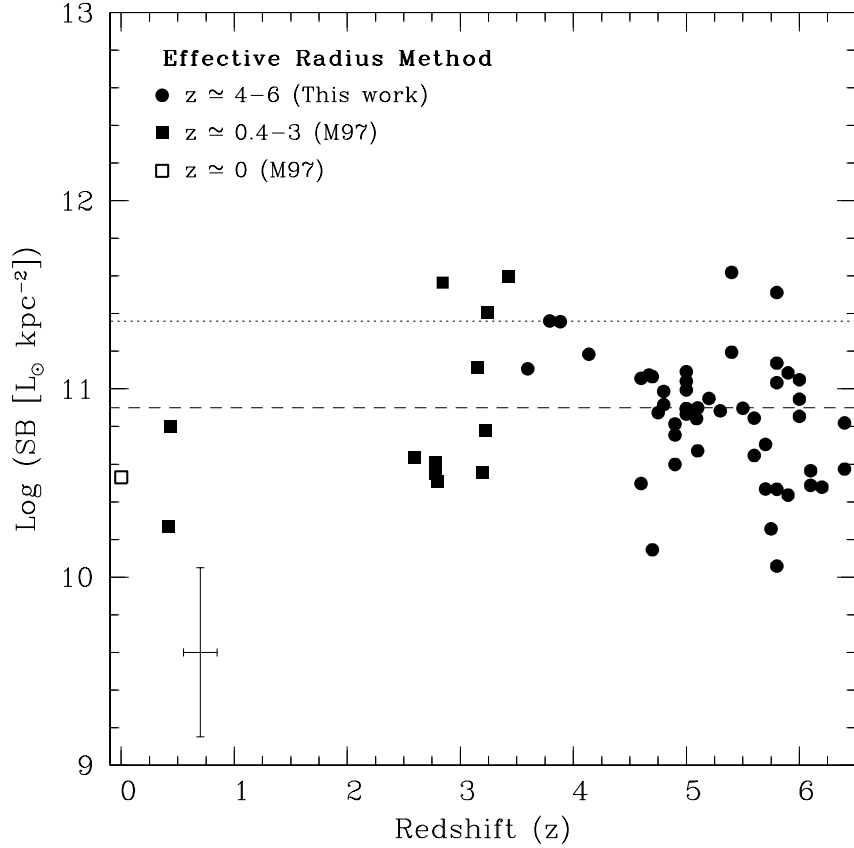


Fig. 4.— Bolometric effective surface brightness ($L_{\odot}^{\text{bol}} \text{ kpc}^{-2}$) as a function of redshift. The open square ($z \simeq 0$) is the median measurement of 11 nearby galaxies from M97. The filled squares ($z \simeq 0.4$) are S_e measurements from M97. The filled squares ($z \simeq 3$) are the galaxies from the sample of M97 for which we measured surface brightnesses. The circles are the galaxies in our sample ($z \simeq 4-6$). The dotted and dashed lines correspond to $S_{e,90}$ and $S_{e,50}$ of the combine sample. Uncertainties in $z \simeq 3-6$ surface brightness (due to radii and flux uncertainties) is shown in lower left corner, details are given in § 5.1.

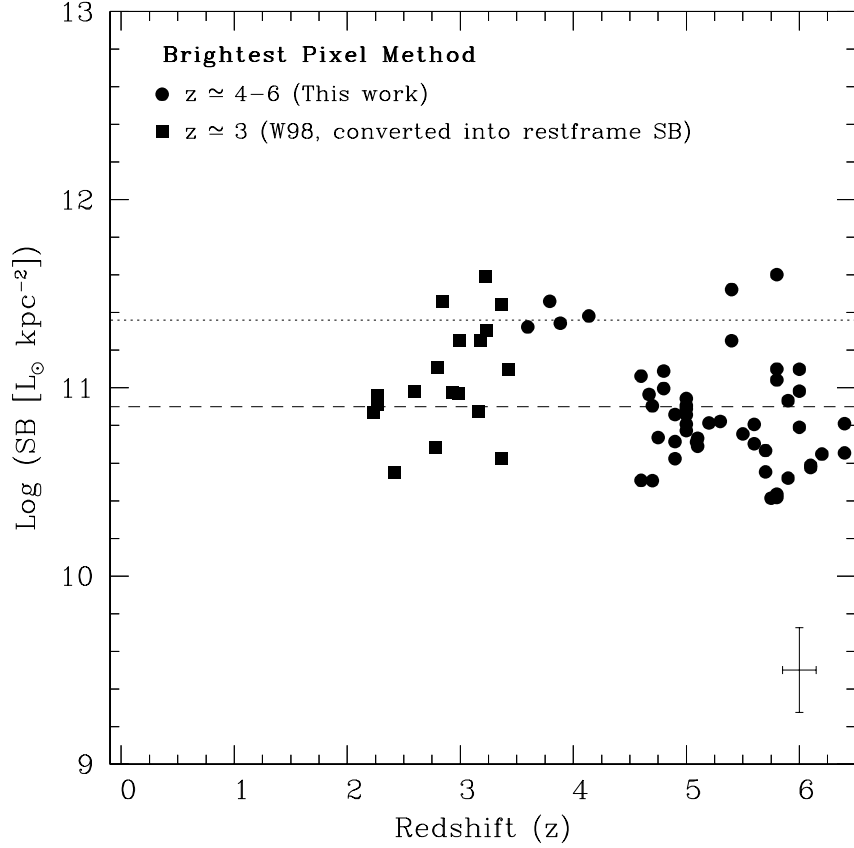


Fig. 5.— Surface Brightness ($L_{\odot}^{\text{UV}} \text{ kpc}^{-2}$) obtained from the brightest pixel of 47 galaxy images at $z \approx 5-6$ and 4 galaxy images at $z \approx 4$. The squares are 18 W98 galaxies. The W98 galaxies had observed surface brightnesses and hence, for proper comparison, we converted observed surface brightnesses to corresponding rest-frame surface brightnesses. The dotted and dashed lines correspond to $S_{bp,90}$ and $S_{bp,50}$ of the combine sample. Uncertainties in surface brightness (due to flux uncertainties only) is shown in lower right corner, details are given in § 5.1.